# Time-dependent magnetotransport of a wave packet in a quantum wire with embedded quantum dots

Gunnar Thorgilsson,[1] Chi-Shung Tang,[2,3,*] and Vidar Gudmundsson[1,†]
[1]*Science Institute, University of Iceland, Dunhaga 3, IS-107 Reykjavik, Iceland*
[2]*Research Center for Applied Sciences, Academia Sinica, Taipei 11529, Taiwan*
[3]*Department of Mechanical Engineering, National United University, Miaoli 36003, Taiwan*
(Received 1 August 2007; revised manuscript received 11 October 2007; published 15 November 2007)

We consider wave packet propagation in a quantum wire with either an embedded antidot or an embedded parallel double open quantum dot under the influence of a uniform magnetic field. The magnetoconductance and the time evolution of an electron wave packet are calculated based on the Lippmann-Schwinger formalism. This approach allows us to look at arbitrary embedded potential profiles and illustrate the results by performing computational simulations for the conductance and the time evolution of the electron wave packet through the quantum wire. In the double-dot system, we observe a long-lived resonance state that enhances the spatial spreading of the wave packet, and quantum skippinglike trajectories are induced when the envelop function of the wave packet covers several subbands in appropriate magnetic fields.

DOI: 10.1103/PhysRevB.76.195314 PACS number(s): 72.10.−d, 73.21.Hb, 73.23.−b, 75.47.−m

## I. INTRODUCTION

Recent progress in nanotechnology enables us to fabricate various types of quantum systems embedded in nanostructures in which the charge carriers behave coherently.[1] Electronic transport in these mesoscopic or nanoscopic size systems is phase coherent, and the universal quantization of the dc conductance is one of the well-known features that was measured in various semiconductor structures.[2] The low-temperature behavior of the conducting electrons becomes dominated by quantum interference effects. For example, a single impurity allows the electrons to make coherent elastic intersubband transitions forming quasibound states nearby the threshold of a subband bottom.[3] One of the advantages of electronic transport is its tunability by applying external magnetic fields.[4–10] Transport properties are affected by the nature of current-carrying states in the leads connecting these structures to electron reservoirs. The electronic transport under influence of an external magnetic field has been utilized in several aspects such as probing impurities in nanostructures under depleted conditions,[7] studying magnetoconductance fluctuations,[8] imaging magnetic focusing of coherent electron waves,[9] and realizing chiral coherent quantum circuits.[10]

One of the typical and significant issues in mesoscopic and nanoscopic systems is time-dependent transport.[11–16] A microelectronic system driven by an external time-dependent potential allows charge carriers to make coherent inelastic scattering. A number of time-dependent transport features have been investigated such as time-dependent quasibound states,[11] nonadiabatic quantum charge pumping,[12,13] current-driven oscillations for nanomechanical rectifiers,[14] and charged particle motion in quantum rings.[15,16] Blumenthal *et al.* demonstrated that the pumped current of hundred picoamperes can be generated and is proportional to the pumping frequency up to 3 GHz.[13] Szafran and Peeters performed time-dependent simulation exploring the electron wave packet trajectories in an open quantum ring by considering the transport in the lowest subband and neglecting inelastic scattering effects.[15] They also suggested an experimental setup in order to measure the Lorentz-force-induced asymmetry in the Aharonov-Bohm effect in a three-terminal semiconductor quantum ring.[17] Considerably earlier, Ancilotto *et al.* used numerical methods to explore the time-dependent tunneling of a Gaussian wave packet through a thick homogeneous barrier in a transverse magnetic field[18] and subsequently used the model to analyze the lifetime of the resonant state formed in a double barrier system.[19]

In the present work, our purpose is to elucidate how the embedded quantum dots in a uniform perpendicular magnetic field affect the transport characteristics of the electron wave packet in a broad ballistic two-terminal quantum wire system. By transforming the embedded potential as well as the scattering wave function into a momentum-coordinate mixed representation,[20] we demonstrate that the wave packet transmission probability and the conductance can be obtained using the Lippmann-Schwinger method.[21] In order to understand in detail, we shall consider embedded antidot and double-dot systems in different magnetic fields for comparison. In magnetic fields, the propagating wave packet states are shifted to the sample boundaries due to the Lorentz force. Detailed information on the embedded nanostructures represents a key to the understanding of various features of the magnetotransport of a wave packet.

The present paper is organized as follows. Section II describes wave packet magnetotransport in a nanostructure embedded quantum wire. In Sec. III, we examine wave packet propagation of the quantum wire with embedded quantum dots and the robustness of the resonance features in appropriate magnetic fields. Concluding remarks and possible future directions are summarized in Sec. IV.

## II. THEORETICAL MODEL

The system under investigation is a two-dimensional quantum wire containing an embedded nanostructure penetrated by a perpendicular magnetic field $\mathbf{B}=B\hat{\mathbf{z}}$. The quantum wire lies in the $x$-$y$ plane, which is assumed to be con-

 

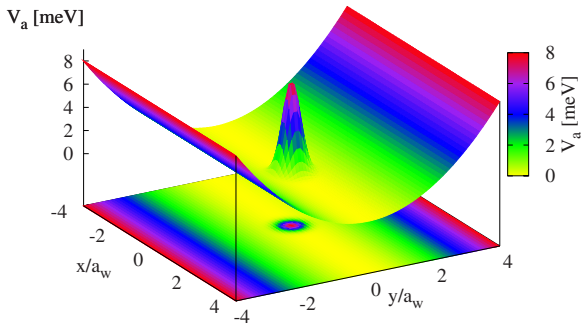


FIG. 1. (Color online) Schematic view of an antidot embedded in a two-terminal quantum wire. $V_{a0}=8$ meV, $\beta_a=10^{-2}$ nm$^{-2}$, and $x_a=0$.

fined in the $y$ direction and transport is in the $x$ direction. The wire stretches into infinity in both directions, while the embedded nanostructure is contained in a scattering region of finite length in the middle of the wire. The Hamiltonian of system contains an unperturbed Hamiltonian and a scattering potential describing the embedded quantum dots, namely, $\mathcal{H}=\mathcal{H}_0+V_{\rm sc}(x,y)$. In this work, we shall explore the time-dependent transport phenomena of embedded antidot and parallel double-dot systems.

The considered embedded antidot is defined in the middle of the quantum wire as shown in Fig. 1 and can be described by a Gaussian-type potential

$$V_a(x,y) = V_{a0}\exp\{-\beta_a[(x-x_a)^2+y^2]\}. \tag{1}$$

For performing numerical computation, the antidot related physical parameters are selected as follows: potential height of the antidot $V_{a0}=8$ meV, the potential broadening parameter $\beta_a=10^{-2}$ nm$^{-2}$, and the longitudinal coordinate center $x_a=0$, with $a_w$ being the effective magnetic length of the wire to be defined later.

The parallel double-dot potential under consideration, shown in Fig. 2, is described by a number of Gaussian-type potentials

$$V_d = V_{d0}\exp[-\beta_d(x-x_d)^2]\sum_{\nu=\pm}\exp[-\beta_d(y+\nu y_d)^2]. \tag{2}$$

The strength of the coupling of the two parallel open quantum dots is tunable by the separation parameter $y_d$ and the

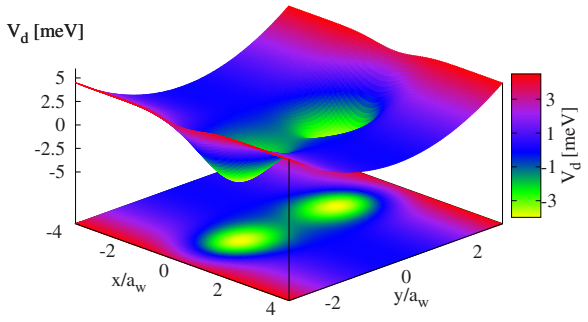


FIG. 2. (Color online) Schematic view of a parallel double-dot embedded in a two-terminal quantum wire. $V_{d0}=-5$ meV, $\beta_d=10^{-3}$ nm$^{-2}$, $x_d=0$, and $y_d=1.5a_w$.

strength of the magnetic field. In our numerical calculation, we shall select the strength of the double quantum dot $V_{d0}=-5$ meV, the broadening parameter $\beta_d=10^{-3}$ nm$^{-2}$, the longitudinal center $x_d=0$, and the transverse off-center parameter $y_d=1.5a_w$ such that the two dots are separated by the distance of $2y_d$.

In the Landau gauge for the vector potential, the unperturbed Hamiltonian can be written as

$$\mathcal{H}_0 = \frac{\hbar^2}{2m^*}\left[-i\nabla - \frac{eB}{\hbar c}y\hat{\mathbf{x}}\right]^2 + V_{\rm conf}(y), \tag{3}$$

where $-e$ and $m^*$ are the charge and the effective mass of an electron, respectively. The confining potential $V_{\rm conf}(y)=\frac{1}{2}m^*\Omega_0^2y^2$ is assumed to be parabolic. Using a mixed momentum-coordinate representation[20] and making Fourier transform in time, the scattering wave function

$$\Psi(x,y,t) = \int_{-\infty}^{\infty}\frac{d\omega}{\sqrt{2\pi}}\int_{-\infty}^{\infty}\frac{dp}{\sqrt{2\pi}}e^{i(px-\omega t)}\tilde{\Psi}(p,y,\omega) \tag{4}$$

can be separated into the coefficient functions $\varphi_n$ and the shifted harmonic-oscillator-type eigenfunctions $\Phi_n$ for the wire, namely, $\tilde{\Psi}(p,y,\omega)=\Sigma_n\varphi_n(p,\omega)\Phi_n(y-y_p)$, where the shifting center $y_p=pa_w^2\omega_c/\Omega_w$ is momentum dependent. In the absence of magnetic field, this shifting center is identically zero. The effective magnetic length of the wire $a_w=\hbar/m^*\Omega_w$ is related to the effective cyclotron frequency $\Omega_w=\sqrt{\Omega_0^2+\omega_c^2}$, with $\omega_c=eB/(m^*c)$ being the two-dimensional cyclotron frequency. In the presence of a magnetic field, the quantized electron energy away from the scattering region is given by[4]

$$E_n(p) = E_n^0 + \frac{U_w}{2}(pa_w)^2, \tag{5}$$

where $E_n^0=(n+1/2)E_w$ are the transverse subband energy levels, and the second term denotes the kinetic energy with $U_w=(\hbar\Omega_0)^2/E_w$ and $E_w=\hbar\Omega_w$.

To obtain the coefficient functions $\varphi_n$, one defines the momentum-coordinate space potential $V(p-q,y)$, which is a Fourier transform of the scattering potential $V_{\rm sc}(x,y)$. The overlap integral in the momentum space can thus be expressed as

$$U_{nn'}(p,q)U_w = \int_{-\infty}^{\infty}dy\Phi_{n'}^*(y-y_q)V(p-q,y)\Phi_n(y-y_p), \tag{6}$$

where $U_{nn'}$ is a dimensionless quantity. In the asymptotic region away from the scattering region, the unperturbed Green's function can be expressed of the form $G_n(p,\omega)=\{[k_n(\omega)a_w]^2-(pa_w)^2\}^{-1}$, where the dimensionless wave vector $k_n(\omega)a_w=[(\hbar\omega-E_n^0)/U_w]^{1/2}$ describes the dispersion relation in the asymptotic regions. After some algebra, one can obtain the Lippmann-Schwinger equation in the momentum space,

$$\varphi_n(p,\omega) = \varphi_n^0(p,\omega) + G_n(p,\omega)\int_{-\infty}^{\infty}\frac{dqa_w}{\sqrt{2\pi}}U_{nn'}(p,q)\varphi_{n'}(q), \tag{7}$$

where $\varphi_n^0(p,\omega)=2\pi g_n(p)\delta[\omega-E_n(p)/\hbar]$ is the coefficient function of the asymptotic regions. Therein, the envelope function of the incident wave packet $g_n(p)$ is assumed to contain only positive $p$ values such that the wave packet is injected in the **x** direction. For a given subband $n$, the explicit form of the coefficient function can be expressed in terms of the $T$ matrix,

$$\varphi_n(p,\omega) = \varphi_n^0(p,\omega) + G_n(p,\omega)\sum_{n'}\int_{-\infty}^{\infty}\frac{dqa_w}{\sqrt{2\pi}}T_{nn'}(p,q,\omega)\varphi_{n'}^0(q,\omega), \tag{8}$$

where the $T$ matrix is a solution of the integral equation

$$T_{nn'}(p,q,\omega) = U_{nn'}(p,q) + \sum_m\int_{-\infty}^{\infty}\frac{dka_w}{\sqrt{2\pi}}U_{nm}(p,k)G_m(k,\omega)T_{mn'}(k,q,\omega). \tag{9}$$

Solving this integral equation for the $T$ matrix, one can obtain the coefficient functions $\varphi_n$ for the scattering region and construct the total wave function $\Psi(x,y,t)=\Psi_0(x,y,t)+\Psi_{sc}(x,y,t)$ containing an asymptotic part,

$$\Psi_0(x,y,t) = \sum_n\int_{-\infty}^{\infty}dpg_n(p)\Phi_n(y-y_p)\exp\{i[px-E_n(p)t/\hbar]\}, \tag{10}$$

with $g_n(p)=\delta_{nn'}\exp[-\gamma(p-p_0)^2]$ being the envelop function of the wave packet in momentum space, and a scattering part,

$$\Psi_{sc}(x,y,t) = \sum_{n'}\int_{E_{n'}^0/\hbar}^{\infty}d\omega e^{-i\omega t}\frac{\Omega_w g_{n'}[k_{n'}(\omega)]}{\Omega_0^2|k_n'(\omega)a_w|} \times\sum_n\int_{-\infty}^{\infty}\frac{dpa_w}{\sqrt{2\pi}}G_n(p,\omega)\exp(ipx) \times T_{nn'}(p,k_{n'}(\omega))\Phi_n(y-y_p). \tag{11}$$

The transmission amplitude through the embedded quantum dot system for an electron with energy $E=\hbar\omega$ entering the scattering region from the channel $n$ in the left lead and leaving it via channel $m$ in the right lead that can be expressed in terms of the $T$ matrix is

$$\mathbf{t}_{nm}(\omega) = \delta_{nm} - \frac{i}{2k_m(\omega)}\frac{2m}{\hbar^2}T_{nm}[k_n(\omega),k_m(\omega)]. \tag{12}$$

The conductance, according to the framework of multichannel Landauer-Büttiker formalism,[22] is written as

$$G = G_0\,\mathrm{Tr}[\mathbf{t}_{nm}^{\dagger}(\omega)\mathbf{t}_{nm}(\omega)], \tag{13}$$

where $G_0=2e^2/h$ is the universal conductance quantum and $\mathbf{t}_{nm}$ is evaluated at the Fermi energy. All the incident and scattered propagating modes have to be taken into account.

## III. NUMERICAL RESULTS

To investigate the magnetotransport properties of wave packet propagation in a nanostructure system embedded in a broad wire under a perpendicular magnetic field, we select the confinement parameter $\hbar\Omega_0=1$ meV. In our numerical calculation, the magnetic field strengths are selected as $B=0.5$ and 1.0 T with corresponding effective magnetic lengths $a_w=29.3$ and 23.9 nm, respectively. We assume that the quantum wire is fabricated in a high-mobility GaAs-$Al_xGa_{1-x}As$ heterostructure such that the effective Rydberg energy $E_{Ryd}=5.92$ meV and the Bohr radius $a_B=9.79$ nm. Below, we shall explore the dynamic motion of the electron wave packet in a quantum wire under an applied perpendicular magnetic field with either an embedded antidot or an embedded double open quantum dot.

### A. Embedded antidot

Earlier work considering magnetotransport in an antidot was carried out by assuming that magnetic field is so strong that only the lowest Landau level is occupied.[23] The antidot can be formed by producing a potential hill with gates[24] and behaves effectively like an artificial quantum impurity. It is thus warranted to devote further effort in developing numerical techniques in order to analyze the behavior of the electron wave packet propagation in a quantum wire with an embedded antidot in a tunable magnetic field.

Since the effective magnetic length $a_w$ is a function of magnetic field, we thus select the envelop parameters of the wave packet in the momentum space as $p_0=1.2a_w^{-1}$ and $\gamma=2.0a_w^2$ for $B=0.5$ T and $p_0=2.0a_w^{-1}$ and $\gamma=1.0a_w^2$ for $B=1.0$ T, such that the wave packets are of similar shapes in momentum space as shown by the dotted blue curve in Fig. 3. The incident wave packet is selected to have contributions from the lowest subband for clarity. The initial electron envelop function at $t=0$ is a Gaussian wave packet in the momentum space with width $\Delta p_{in}=1/\sqrt{\gamma}$ such that the probability density of the wave packet in the momentum space is reduced by a factor of $1/\sqrt{e}$.

The energy dependences of the conductance for the traveling wave packet in an ideal wire and an antidot embedded wire are depicted in Fig. 3 by the dashed green and the solid red curves, respectively. The general feature in Fig. 3 is that the conductance is suppressed in the low kinetic energy regime but approaches the conductance of the ideal wire in the high kinetic energy regime. This is because the electron waves with lower kinetic energy are easier to be backscattered by the embedded antidot. For the case of $B=0.5$ T, the conductance manifests a smooth transition region in the lowest subband ($n=0$). Low kinetic energy blocking phenomenon is significant at the third and the fifth conductance plateaus. However, in the second and the fourth plateaus, the Lorentz force pushes transversely the electron wave packet

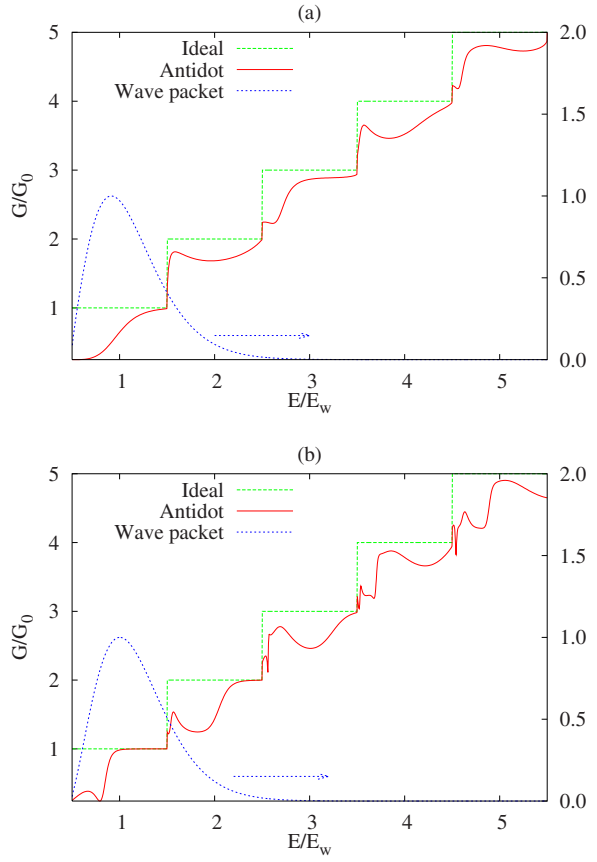


FIG. 3. (Color online) Energy dependence of the conductance in an ideal wire (dashed green), the conductance in an antidot embedded wire (solid red), and the envelop function of the wave packet in momentum space (dotted blue) for the cases of (a) $B=0.5$ with wave packet parameters $p_0=1.2a_w^{-1}$ and $\gamma=2.0a_w^2$ and (b) $B=1.0$ T with wave packet parameters $p_0=2.0a_w^{-1}$ and $\gamma=1.0a_w^2$. The other parameters are the same as in Fig. 1.

with intermediate kinetic energy and hence suppresses slightly the conductance plateaus.

For the case of $B=1.0$ T, the conductance in the lowest subband region exhibits clear transition between the backward and the forward propagating energy regimes at around $E\simeq E_w$. A dip structure is clearly found at $E\simeq 0.79E_w$ that corresponds to a short-lived quasibound state with negative binding energy. Such a dip structure becomes broader valley structure at higher subbands shifted slightly to the higher energy. This broadening indicates a shorter dwell time of the localized state at higher subbands. Sharp dip structures at $E=2.56$, 3.52, and $4.54E_w$ demonstrate the formation of quasibound states with negative binding energy.[25]

In Fig. 4, we show the time evolution of the wave packet traveling through the quantum wire with an embedded antidot for the case of $B=0.5$ T. Before the electron wave packet arrives at the scattering region, the wave packet center is shifted slightly in transverse direction to $y\approx 0.8a_w$ due to the Lorentz force induced by the penetrating magnetic field as shown in Fig. 4(a) for $t=0$ ps. To estimate the longitudinal width of the incident Gaussian wave packet, it is convenient to define a Gaussian function in the real space $f(x)=e^{-x^2/\gamma}$

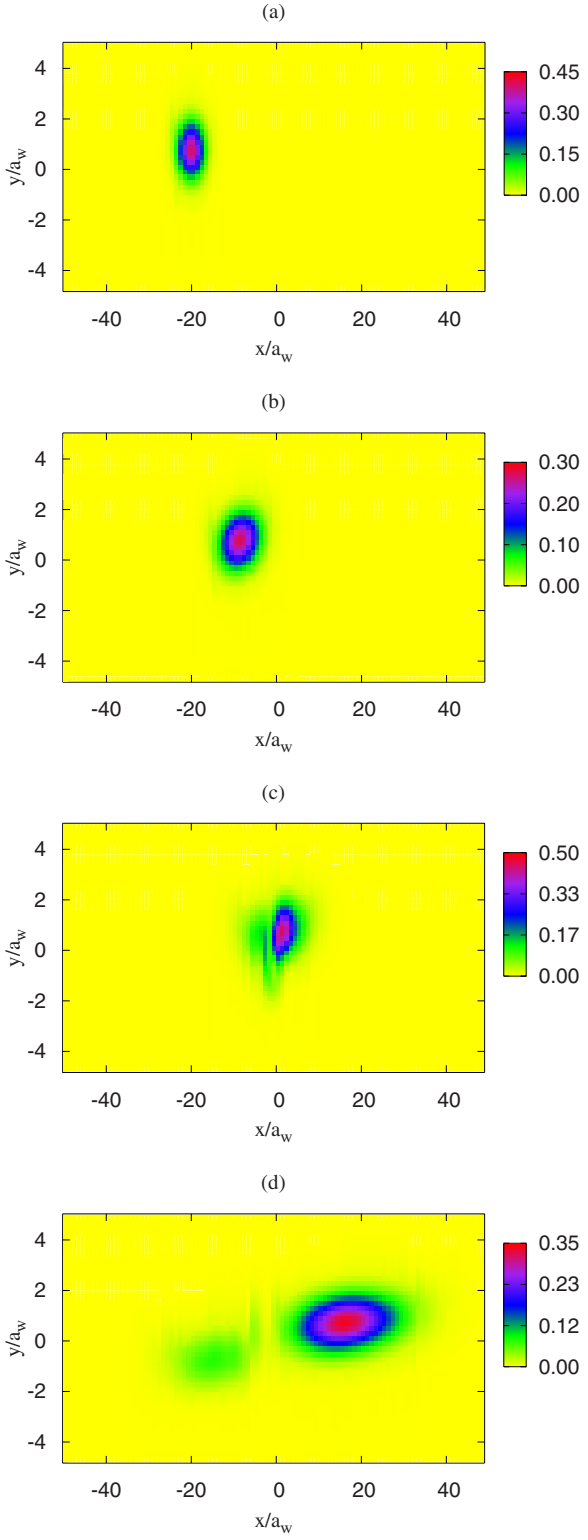


FIG. 4. (Color online) Propagation of the electron wave packet traveling through an embedded antidot for the case of $B=0.5$ T at time $t=$(a) 0, (b) 8, (c) 15, and (d) 28 ps. The other parameters are the same as in Fig. 1.

with width $\Delta x$ such that $x$ varies from 0 to $\pm\Delta x/2$, and $f(x)$ is reduced by a factor of $e^{-1/2}$. By this definition, one can estimate the width of the incident wave packet at $t=0$ being

$\Delta x_{\text{in}}=2\sqrt{\gamma}a_w$ to obtain $\Delta x_{\text{in}}\Delta p_{\text{in}}=2$, which is compatible with the Heisenberg uncertainty relation.

Figure 4(b) shows the time evolution of the wave packet at $t=8$ ps, and it is found that the trajectory of the electron waves with higher kinetic energy is closer to the wire edge due to the magnetic field. Since the higher kinetic energy electron waves contain larger group velocity, the shape of the wave packet is skewed, an effect also seen by Ancilotto *et al.*[19] The electron wave packet is then scattered by the antidot as shown in Fig. 4(c). The electron waves with higher kinetic energy can pass through the antidot but the lower kinetic energy part of the wave packet is reflected. Due to the Lorentz force, the backscattered wave packet is turned around to the lower part of the quantum wire with wave packet center at $y=-0.6a_w$ [see Fig. 4(c)]. For longer evolution time $t=28$ ps, the scattered wave packets become broader and then leave the scattering region, as is shown in Fig. 4(d).

In Fig. 5, we show the time evolution of the wave packet traveling through the quantum wire with an embedded antidot for the case of $B=1.0$ T. Before the electron wave packet arrives at the scattering region, the wave packet has a shifting center at $y\approx 1.8a_w$ due to the Lorentz force as shown in Fig. 5(a) for 0 ps. The wave packet is narrow in the $x$ direction, that is, $\Delta x_{\text{in}}=2a_w$. The electron wave packet is scattered by the antidot at $t=15$ ps, as is shown in Fig. 5(b). The part with higher kinetic energy can pass through the antidot, but the part with lower kinetic energy is predominately reflected. Due to the magnetic field induced Lorentz force, the backscattered wave packet is turned around to the lower part of the quantum wire with wave packet center at $y=-1.2a_w$ at $t=25$ ps [see Fig. 5(c)]. For longer time $t=40$ ps, the scattered wave packets are getting broader—the reflected wave packet has distribution length $\Delta x_{\text{ref}}\approx 10a_w$ and the transmitted wave packet has even broader distribution length $\Delta x_{\text{tran}}\approx 20a_w$, as is shown in Fig. 5(d). The spreading of a wave packet is a quantum diffusion phenomenon, which was utilized for possible application in a quantum kicked rotor system.[26]

In comparison with the incident wave packet in an applied magnetic field $B=1.0$ T, the incident wave packet in $B=0.5$ T has a wider longitudinal profile and a wave packet center closer to the middle of the quantum wire. It turns out that the group velocity of the wave packet for the case of $B=0.5$ T is greater than that of $B=1.0$ T. We would like to mention in passing that for a wave packet with momentum envelop function covering more subbands, the electron wave packet tends to form transversely skippinglike trajectories in both the forward and backward scattered wave packets due to the mode mixing interference between different subbands.

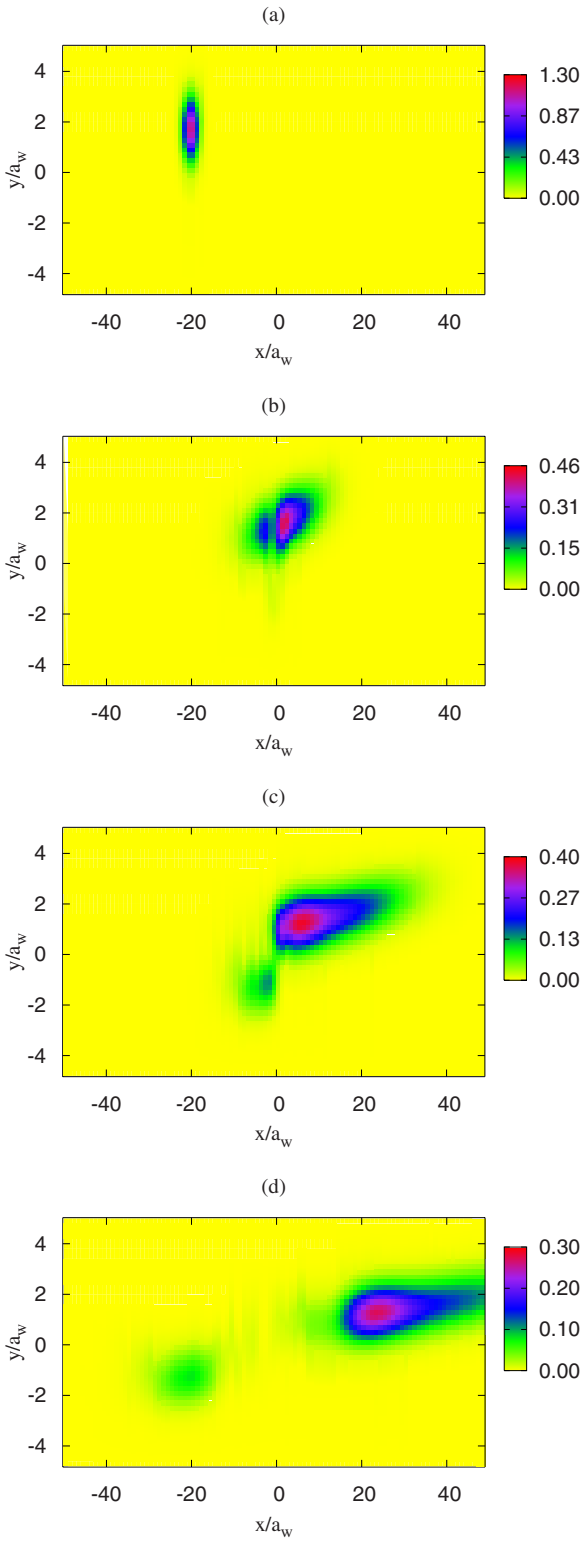


FIG. 5. (Color online) Propagation of the electron wave packet traveling through an embedded antidot for the case of $B=1.0$ T at time $t=$(a) 0, (b) 15, (c) 25, and (d) 40 ps. The other parameters are the same as in Fig. 1.

### B. Embedded parallel double dot

Electronic transport through coupled quantum nanostructures is of fundamental interest for the understanding of coherent resonant and superposition states. By coupling two quantum dots in series[27] or in parallel,[28] a double quantum dot is formed. Quantum transport through such a double-dot system has attracted considerable attention due to its versatility for various applications such as probing entanglement,[29] detecting microwave manipulation of a single electron,[30] analyzing dephasing rate,[31] studying nona-

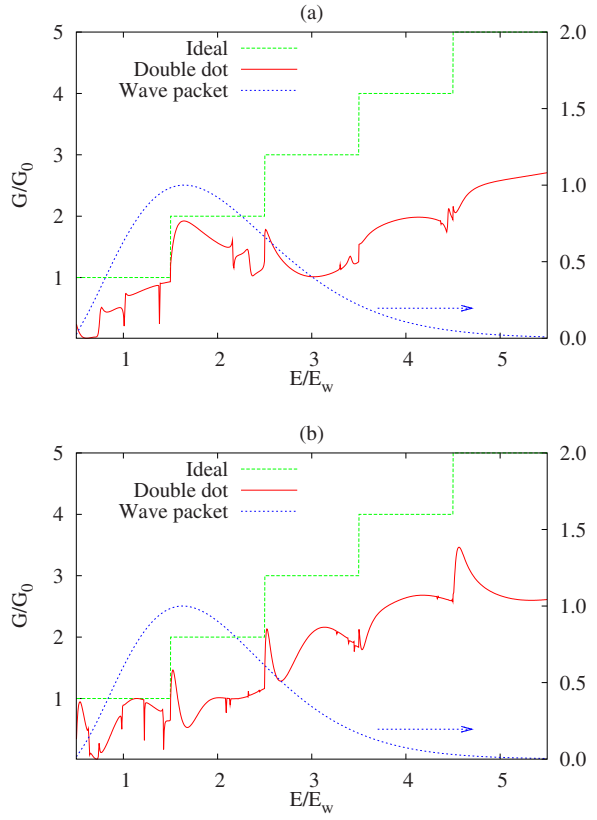


FIG. 6. (Color online) Energy dependence of the conductance in an ideal wire (dashed green), the conductance in a double-dot embedded quantum wire (solid red), and the envelop function of the wave packet in momentum space (dotted blue) for the cases of (a) $B=0.5$ with wave packet parameters $p_0=1.0a_w^{-1}$ and $\gamma=2.0a_w^2$ and (b) $B=1.0$ T with wave packet parameters $p_0=3.0a_w^{-1}$ and $\gamma=0.5a_w^2$. The other parameters are the same as in Fig. 2.

diabatic transport under irradiation,[32] and readout of the coherent superposition of trajectories.[33] The interdot coupling strength can be experimentally varied using gate electrodes.[28,34]

Earlier works considering electronic transport in double quantum dot systems were carried out using the Anderson-type hopping model by assuming that the system is isolated with weak coupling to the leads.[35] Our previous work has devoted effort in developing numerical computation of magnetotransport in a transversely hill-separated parallel double open quantum dot system with strong coupling to the leads.[36] It is thus appropriate to analyze the propagation behavior of the electron wave packet in a quantum wire with an embedded parallel double open quantum dot to get better insight into the dynamical properties.

In Fig. 6, we show the energy dependence of the conductance in an ideal wire (dashed green), the conductance in a double-dot embedded quantum wire (solid red), and the envelop function of the wave packet in momentum space (dotted blue) for the cases of (a) $B=0.5$ T and (b) $B=1.0$ T. We select the envelop parameters of the wave packet in the momentum space as packet center $p_0=1.0a_w^{-1}$ and $\gamma=2.0a_w^2$ for $B=0.5$ T and $p_0=3.0a_w^{-1}$ and $\gamma=0.5a_w^2$ for $B=1.0$ T, such that the wave packets are of similar shapes in momentum space.

For the case of $B=0.5$ T, shown in Fig. 6(a), we see that a perfect conductance gap formed at the kinetic energy regime $(0.53<E/E_w<0.73)$ of the first subband. This fact indicates that the embedded double-dot system may be applicable as a quantum switch. The conductance gap is formed due to the cyclotron motion of electron wave between the two parallel dots. Fano line shapes in conductance at energies $E=1.01$ and $2.37E_w$ manifest the quantum interference feature of the wave packet between the part forming quasibound states inside the double-dot system and the part with straight transmission. Furthermore, a sharp dip structure in conductance at energy $E=1.38E_w$ indicates the formation of a quasibound state below the second subband threshold in the lead. The transport properties of electron waves in the second subband are very different to that in the first subband. The overall feature is that the low kinetic energy electron exhibits higher conductance. The strong suppression in conductance at higher subband implies the better interdot coupling enhancing backscattering.

Figure 6(b) shows the energy dependence of conductance for the case of $B=1.0$ T. The gap feature in conductance at the low kinetic energy of the first subband is narrower than that induced by the magnetic field $B=0.5$ T. The dip structure in conductance related to the formation of quasibound state at around the energy $E=E_w$ is almost the same as the case of $B=0.5$ T, but the dip structure at higher energy in the first subband is shifted toward the lower energy. A new clear sharp dip structure is formed just below the threshold of the second subband. Since the wave function of the electrons occupying the second subband in $B=1.0$ T fits the geometry of the double dot system, the electron wave thus favors to turn around through the double-dot, and then the conductance is strongly suppressed. The conductance at energies higher than the third subband threshold for the case of $B=1.0$ T is a little higher than that of $B=0.5$ T.

Figure 7 demonstrates the snapshots of the electron wave packet propagation through an embedded parallel double-dot system for the case of $B=0.5$ T at the time $t=$(a) 0, (b) 9, (c) 25, and (d) 38 ps. At time $t=0$ ps, we see that the incident wave packet has a compact longitudinal distribution $\Delta x_{\text{in}}=2\sqrt{2}a_w$ with height of 1.5. In Fig. 7(b), at $t=9$ ps, the electron wave packet arrives at the upper open dot and forms a clear quasibound state with packet height of 2.0. At this moment, both the backward reflection and the forward transmission are blocked by the double-dot system.

During the time evolution $0<t<9$ ps, the higher energy part of the electron wave packet is closer to the upper boundary and traveling faster than the lower energy part of the wave packet. This makes the electron wave packet to skew with a clockwise rotation. Before being scattered by the double-dot system, the spreading effect proceeds slowly. When the electron wave packet is scattered by the double-dot system, the forward scattered wave packet exhibits faster spreading in the longitudinal direction manifesting a long-tail behavior caused by the slow release of the probability by the long-lived resonance state.

In Fig. 7(c), at the time 25 ps, part of the wave packet is clearly coupled to the lower dot, although part of the wave packet has been forward scattered showing skippinglike trajectories and traveling into the right asymptotic region. The

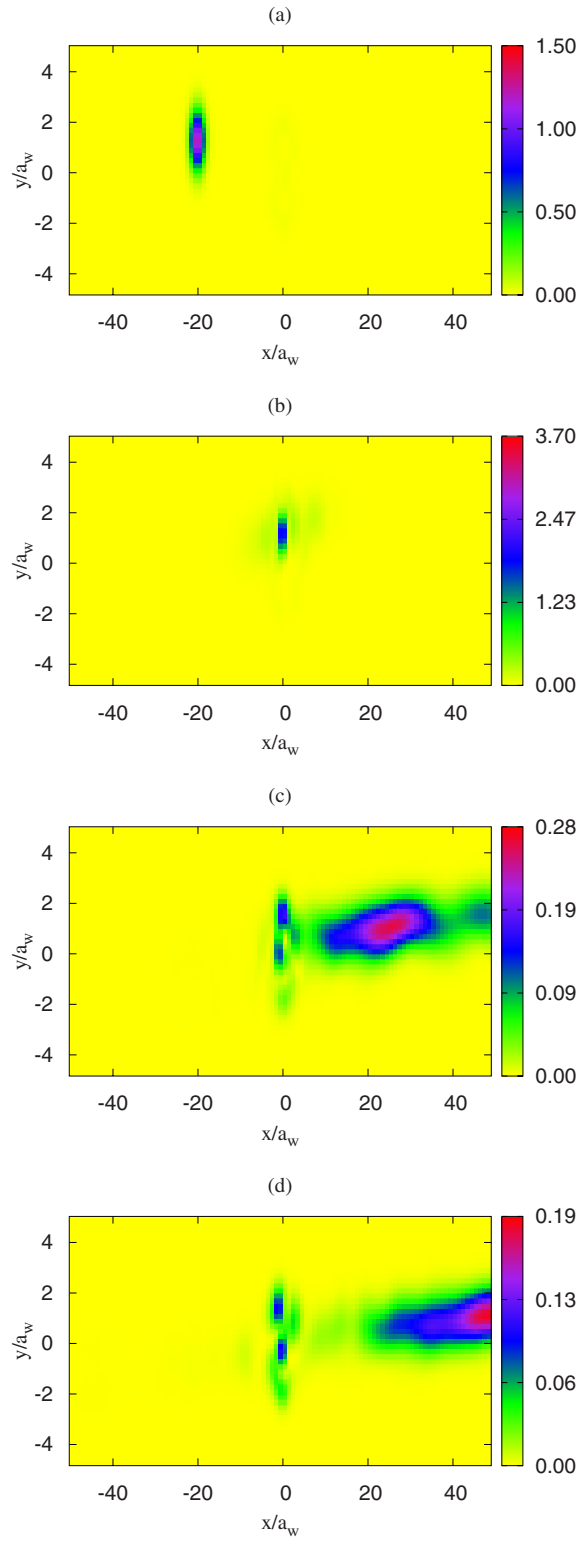


FIG. 7. (Color online) Propagation of the electron wave packet traveling through an embedded parallel double-dot system for the case of $B=0.5$ T at time $t=$(a) 0, (b) 9, (c) 25, and (d) 38 ps. The other parameters are the same in as Fig. 2.

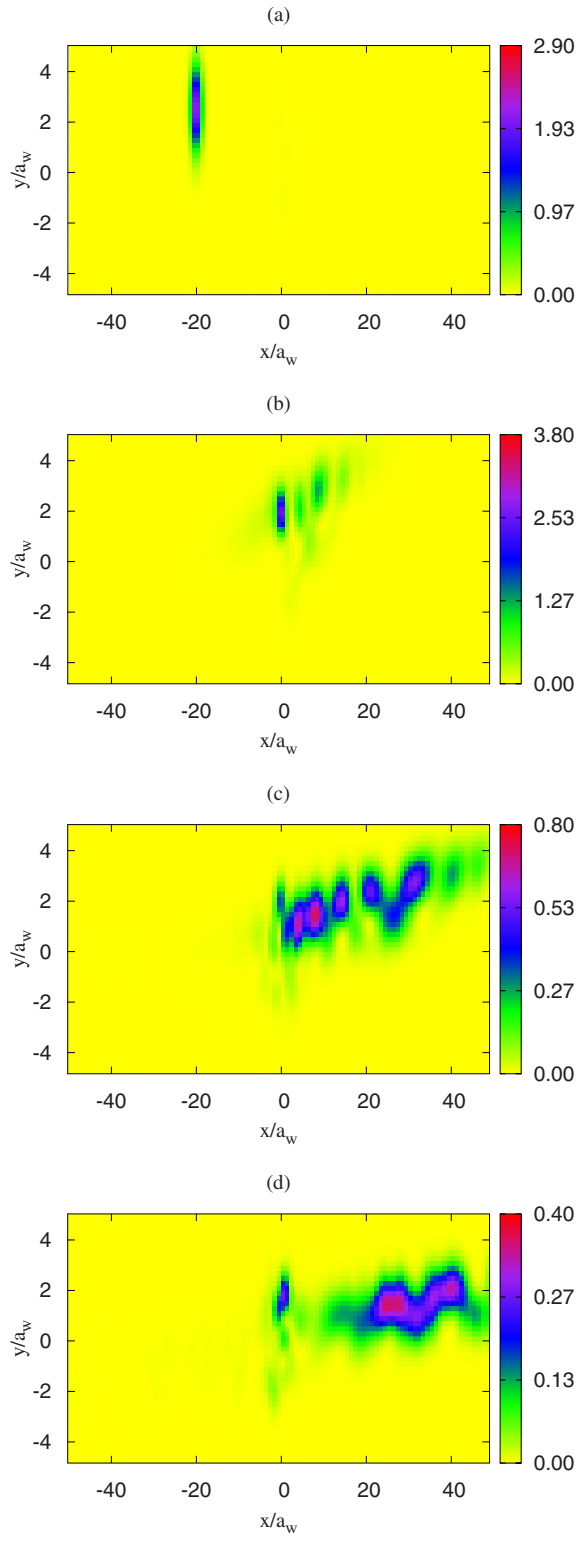


FIG. 8. (Color online) Propagation of the electron wave packet traveling through an embedded parallel double-dot system for the case of $B=1.0$ T at time $t=$(a) 0, (b) 11, (c) 21, and (d) 40 ps. The other parameters are the same as in Fig. 2.

skippinglike behavior implies a significant intersubband mixing due to the broad wave packet distribution in the momentum space. At $t=38$ ps, the longitudinal distribution of the forward scattered wave packet is getting broader, and the localized part remains in the double-dot region with approximately a half packet height of the localized state formed at

$t=9$ ps as shown in Fig. 7(b). We would like to mention in passing that the reflection wave packet takes more time to emerge than the transmission wave packet due to the formation of the quasibound states in the double-dot embedded system.

We show, in Fig. 8, the snapshots of the electron wave packet propagation through an embedded parallel double-dot system for the case of $B=1.0$ T at the time $t=$(a) 0, (b) 11, (c) 21, and (d) 40 ps. It is shown in Fig. 8(a) that, at time $t=0$ ps, the incident wave packet has a compact longitudinal distribution $\Delta x_{\text{in}}=\sqrt{2}a_w$ with probability density height of 1.2. A clear localized quasibound state feature is found at $t=9$ ps, as is shown in Fig. 8(b). The height of the probability density of the localized state is twice the height of the initial wave packet. At this moment, the backward reflection is blocked and the forward transmission is relatively low.

The wave packet propagation at the moment $t=21$ ps is depicted in Fig. 8(c). The forward scattered wave packet exhibits rich and robust transport behavior. Not only the skippinglike wave packet flight is found, but also an interference feature attributed to the intersubband mixing is significantly manifested. At time $t=40$ ps shown in Fig. 8(d), the skippinglike trajectory is still significant but the interference feature is suppressed. In addition, the interdot coupling of the wave packet in $B=1.0$ T is weaker than that in $B=0.5$ T due to the stronger Lorentz force enhancing off-center shifting. The localized state for the case of $B=0.5$ T covers two quantum dots, whereas the localized state for the case of $B=1.0$ T is mainly in the upper dot. This implies that the 0.5 T magnetic field fits better to the length scales of the double-dot system.

## IV. CONCLUDING REMARKS

In this work, we have developed a theoretical model by implementing the Lippmann-Schwinger formalism to demonstrate and elucidate the transport properties of a Gaussian-type electron wave packet traveling through a quantum wire with embedded quantum dots under a homogeneous perpendicular magnetic field. The magnetic field induces Lorentz force, which enriches the dynamics of electron wave packet propagation. We have found that quantum skippinglike oscillation trajectory of a wave packet is induced in an appropriate magnetic field when the wave packet envelop function covers the lowest two subbands. This is a quantum forerunner to the well-known skipping orbit motion of classical particles.

For the case of an embedded antidot, the electron wave packet has been considered with momentum envelop covering the lowest two subbands. The wave packet propagation exhibiting non-skipping-like trajectories implies that the significance of the wave packet propagation stays in the lowest subband. The part of the wave packet with high kinetic energy tends to go through the antidot system, but the part with low kinetic energy is backscattered by the scattering region. Quasibound state features with negative binding energies have also been seen to play an active role in the scattering process.

For the case of embedded double quantum dot, we have found a robust trapping effect of the electronic wave packet moving into the double-dot system and forming localized states. If there are several bound states, the electrons make multiple scattering in the coupled double quantum dot resulting in a superposition of these bound states, exhibiting oscillating behavior in the double-dot system. The parallel double-dot system enables the electron wave packet performing resonant coupling between two dots in an appropriate magnetic field and then allows electron wave packet performing interedge backscattering.

We have referred to resonance structures in the conductance as either dips in the conductance due to the formation of quasibound states or simply as Fano resonances.[37] In fact, both are Fano resonances, and the line shape depends on the relative weight of the continuum and the resonance channel. Recently, this aspect has been clearly addressed by Schánchez and Serra for a system with local Rasbha spin-orbit interaction.[38]

The coherent motion of electron waves through open nanostructures in a penetrating magnetic field may offer promising approaches to semiconductor spintronics[39] and controlling the dynamics of coherent quantum states for quantum information processing.[40] To explore these directions, we need to track the motion of electron waves in an applied magnetic field. The cooled scanning probe microscope renders the possibility of imaging the electron wave trajectories by using the scanning tip as a movable gate.[41] Very recently, quantum dot embedded mesoscopic system has been utilized for the coherent probing of excited quantum dot states.[42] We hope that our paper will stimulate experimental interest to nanostructure embedded quantum systems in the strong coupling regime, which may provide a useful tool for the dynamical quantum manipulation of charged carriers.

## ACKNOWLEDGMENTS

The authors acknowledge financial support from the Research and Instruments Funds of the Icelandic State, the Research Fund of the University of Iceland, the Icelandic Science and Technology Research Programme for Postgenomic Biomedicine, Nanoscience and Nanotechnology, the National Science Council of Taiwan, and the National Center for Theoretical Sciences, Tsing Hua University, Hsinchu, Taiwan. C.-S.T. is grateful to the National Center for High-Performance Computing in Taiwan and the University of Iceland for the use of computational facilities.

*cstang@nuu.edu.tw
†vidar@raunvis.hi.is

[1] See, for example, M. Law, J. Goldberger, and P. Yang, Annu. Rev. Mater. Res. **34**, 83 (2004); J. Noborisaka, J. Motohisa, S. Hara, and T. Fukui, Appl. Phys. Lett. **87**, 093109 (2005).

[2] B. J. van Wees, H. van Houten, C. W. J. Beenakker, J. G. Williamson, L. P. Kouwenhoven, D. van der Marel, and C. T. Foxon, Phys. Rev. Lett. **60**, 848 (1988); S. J. Koester, C. R. Bolognesi, M. J. Rooks, E. L. Hu, and H. Kroemer, Appl. Phys. Lett. **62**, 1373 (1993); G. Scappucci, L. Di Gaspare, E. Giovine, A. Notargiacomo, R. Leoni, and F. Evangelisti, Phys. Rev. B **74**, 035321 (2006).

[3] C. S. Chu and R. S. Sorbello, Phys. Rev. B **40**, 5941 (1989); P. F. Bagwell, *ibid.* **41**, 10354 (1990); J. H. Bardarson, I. Magnusdottir, G. Gudmundsdottir, C. S. Tang, A. Manolescu, and V. Gudmundsson, *ibid.* **70**, 245308 (2004).

[4] J. F. Weisz and K.-F. Berggren, Phys. Rev. B **40**, 1325 (1989); C. S. Tang and V. Gudmundsson, *ibid.* **74**, 195323 (2006); V. Gudmundsson and C. S. Tang, *ibid.* **74**, 125302 (2006).

[5] O. Olendski and L. Mikhailovska, Phys. Rev. B **72**, 235314 (2005).

[6] M. C. Rogge, F. Cavaliere, M. Sassetti, R. J. Haug, and B. Kramer, New J. Phys. **8**, 298 (2006).

[7] J. J. Koonen, H. Buhmann, and L. W. Molenkamp, Phys. Rev. Lett. **84**, 2473 (2000).

[8] A. Löfgren, C. A. Marlow, T. E. Humphrey, I. Shorubalko, R. P. Taylor, P. Omling, R. Newbury, P. E. Lindelof, and H. Linke, Phys. Rev. B **73**, 235321 (2006).

[9] K. E. Aidala, R. E. Parrott, T. Kramer, E. J. Heller, R. M. Westervelt, M. P. Hanson, and A. C. Gossard, Nat. Phys. **3**, 464 (2007).

[10] J. Gabelli, G. Fève, J.-M. Berroir, B. Placais, A. Cavanna, B. Etienne, Y. Jin, and D. C. Glattli, Science **313**, 499 (2006); J. Gabelli, G. Fève, T. Kontos, J.-M. Berroir, B. Placais, D. C. Glattli, B. Etienne, Y. Jin, and M. Büttiker, Phys. Rev. Lett. **98**, 166806 (2007).

[11] C. S. Tang and C. S. Chu, Phys. Rev. B **53**, 4838 (1996); Physica B **254**, 178 (1998); Phys. Rev. B **60**, 1830 (1999); Physica B **292**, 127 (2000); C. S. Tang, Y. H. Tan, and C. S. Chu, Phys. Rev. B **67**, 205324 (2003); B. H. Wu and J. C. Cao, *ibid.* **73**, 245412 (2006).

[12] C. S. Tang and C. S. Chu, Solid State Commun. **120**, 353 (2001); S. W. Chung, C. S. Tang, C. S. Chu, and C. Y. Chang, Phys. Rev. B **70**, 085315 (2004); J. Bylander, T. Duty, and P. Delsing, Nature (London) **434**, 361 (2005).

[13] M. D. Blumenthal, B. Kaestner, L. Li, S. Giblin, T. J. B. M. Janssen, M. Pepper, D. Anderson, G. Jones, and D. A. Ritchie, Nat. Phys. **3**, 343 (2007).

[14] A. G. Mal'shukov, C. S. Tang, C. S. Chu, and K. A. Chao, Phys. Rev. Lett. **95**, 107203 (2005); C. C. Kaun and T. Seideman, *ibid.* **94**, 226801 (2005); F. Pistolesi and R. Fazio, New J. Phys. **8**, 113 (2006).

[15] B. Szafran and F. M. Peeters, Phys. Rev. B **72**, 165301 (2005).

[16] T. Okunishi, Y. Ohtsuka, M. Muraguchi, and K. Takeda, Phys. Rev. B **75**, 245314 (2007); W. H. Kuan, C. S. Tang, and C. H. Chang, *ibid.* **75**, 155326 (2007); P. G. Luan and C. S. Tang, J. Phys.: Condens. Matter **19**, 176224 (2007).

[17] B. Szafran and F. M. Peeters, Europhys. Lett. **70**, 810 (2005).

[18] F. Ancilotto, A. Selloni, L. F. Xu, and E. Tosatti, Phys. Rev. B **39**, 8322 (1989).

[19] F. Ancilotto, A. Selloni, and E. Tosatti, Phys. Rev. B **40**, 3729 (1989).

[20] S. A. Gurvitz, Phys. Rev. B **51**, 7123 (1995); V. Gudmundsson, Y. Y. Lin, C. S. Tang, V. Moldoveanu, J. H. Bardarson, and A. Manolescu, *ibid.* **71**, 235302 (2005).

[21] See, e. g., M. Di Ventra and N. D. Lang, Phys. Rev. B **65**, 045402 (2001).

[22] M. Büttiker, Y. Imry, R. Landauer, and S. Pinhas, Phys. Rev. B **31**, 6207 (1985); Y. Imry and R. Landauer, Rev. Mod. Phys. **71**, S306 (1999).

[23] D. Sanchez and M. Büttiker, Phys. Rev. Lett. **93**, 106802 (2004).

[24] G. Kirczenow, A. S. Sachrajda, Y. Feng, R. P. Taylor, L. Henning, J. Wang, P. Zawadzki, and P. T. Coleridge, Phys. Rev. Lett. **72**, 2069 (1994); M. Kataoka, C. J. B. Ford, M. Y. Simmons, and D. A. Ritchie, *ibid.* **89**, 226803 (2002).

[25] V. Gudmundsson, C. S. Tang, and A. Manolescu, Phys. Rev. B **72**, 153306 (2005).

[26] J. Zhong, R. B. Diener, D. A. Steck, W. H. Oskay, M. G. Raizen, E. W. Plummer, Z. Zhang, and Q. Niu, Phys. Rev. Lett. **86**, 2485 (2001).

[27] For a general overview, see, e. g., W. G. van der Wiel, S. D. Franceschi, J. M. Elzerman, T. Fujisawa, S. Tarucha, and L. P. Kouwenhoven, Rev. Mod. Phys. **75**, 1 (2003).

[28] J. C. Chen, A. M. Chang, and M. R. Melloch, Phys. Rev. Lett. **92**, 176801 (2004).

[29] D. Loss and E. V. Sukhorukov, Phys. Rev. Lett. **84**, 1035 (2000); H. Schomerus and J. P. Robinson, New J. Phys. **9**, 67 (2007).

[30] J. R. Petta, A. C. Johnson, C. M. Marcus, M. P. Hanson, and A. C. Gossard, Phys. Rev. Lett. **93**, 186802 (2004).

[31] M. Elhassan, J. P. Bird, R Akis, D. K. Ferry, T. Ida, and K. Ishibashi, J. Phys.: Condens. Matter **17**, L351 (2005).

[32] W. J. M. Naber, T. Fujisawa, H. W. Liu, and W. G. van der Wiel, Phys. Rev. Lett. **96**, 136807 (2006).

[33] A. N. Jordan, A. N. Korotkov, and M. Büttiker, Phys. Rev. Lett. **97**, 026805 (2006).

[34] N. J. Craig, J. M. Taylor, E. A. Lester, C. M. Marcus, M. P. Hanson, and A. C. Gossard, Science **304**, 565 (2004).

[35] M. N. Kiselev, K. Kikoin, and L. W. Molenkamp, Phys. Rev. B **68**, 155323 (2003); U. Hartmann and F. K. Wilhelm, *ibid.* **69**, 161309(R) (2004); G. Zaránd, C.-H. Chung, P. Simon, and M. Vojta, Phys. Rev. Lett. **97**, 166802 (2006).

[36] C. S. Tang, W. W. Yu, and V. Gudmundsson, Phys. Rev. B **72**, 195331 (2005).

[37] U. Fano, Phys. Rev. **124**, 1866 (1961).

[38] David Sánchez and Llorenç Serra, Phys. Rev. B **74**, 153313 (2006).

[39] I. V. Zozoulenko and M. Evaldsson, Appl. Phys. Lett. **85**, 3136 (2004).

[40] J. Harris, R. Akis, and D. K. Ferry, Appl. Phys. Lett. **79**, 2214 (2001).

[41] M. A. Topinka, B. J. LeRoy, S. E. J. Shaw, E. J. Heller, R. M. Westervelt, K. D. Maranowski, and A. C. Gossard, Science **289**, 2323 (2000); M. A. Topinka, R. M. Westervelt, and E. J. Heller, Phys. Today **56**(12), 47 (2003).

[42] M. Sigrist, Thomas Ihn, K. Ensslin, M. Reinwald, and W. Wegscheider, Phys. Rev. Lett. **98**, 036805 (2007).